Published in final edited form as:
FASEB J. 2005 February ; 19(2): 298–300. doi:10.1096/fj.04-2549fje.

Plasma membrane calcium ATPase deficiency causes neuronal pathology in the spinal cord: a potential mechanism for neurodegeneration in multiple sclerosis and spinal cord injury

Michael P. Kurnellas[*,†,1], **Arnaud Nicot**[§,1], **Gary E. Shull**[¶], and **Stella Elkabes**[*,†]

[*] Neurology and Neuroscience, UMDNJ-New Jersey Medical School, Newark, NJ 07103

[†] Neurology Service, Veterans Affairs, East Orange, NJ, 07018

[§] INSERM EMI 0350, Hôpital St. Antoine, Paris, France

[¶] Molecular Genetics, Biochemistry and Microbiology, University of Cincinnati, Cincinnati, OH 45267

Abstract

Dysfunction and death of spinal cord neurons are critical determinants of neurological deficits in various pathological conditions, including multiple sclerosis (MS) and spinal cord injury. Yet, the molecular mechanisms underlying neuronal/axonal damage remain undefined. Our previous studies raised the possibility that a decrease in the levels of plasma membrane calcium ATPase isoform 2 (PMCA2), a major pump extruding calcium from neurons, promotes neuronal pathology in the spinal cord during experimental autoimmune encephalomyelitis (EAE), an animal model of MS, and after spinal cord trauma. However, the causal relationship between alterations in PMCA2 levels and neuronal injury was not well established. We now report that inhibition of PMCA activity in purified spinal cord neuronal cultures delays calcium clearance, increases the number of nonphosphorylated neurofilament H (SMI-32) immunoreactive cells, and induces swelling and beading of SMI-32-positive neurites. These changes are followed by activation of caspase-3 and neuronal loss. Importantly, the number of spinal cord motor neurons is significantly decreased in PMCA2-deficient mice and the *deafwaddler*^{2J}, a mouse with a functionally null mutation in the PMCA2 gene. Our findings suggest that a reduction in PMCA2 level or activity leading to delays in calcium clearance may cause neuronal damage and loss in the spinal cord.

Keywords

autoimmune disease; ATP2B2; excitotoxicity; cytoskeleton

Neuronal and axonal dysfunction and loss have increasingly received attention as important contributors to neural decline in various central nervous system (CNS) disorders, including MS and spinal cord trauma. MS is a CNS disease that may initially show a relapsing-remitting course but finally leads to permanent neurological impairment (1,2). Classically, demyelination of structurally intact axons was considered to be the main cause of clinical symptoms and neural deficits in MS. However, recent studies indicate that axonal dysfunction is already evident at the earliest clinical stages of MS, and axonal transection or loss may be the cause of persistent, irreversible disability at later phases of the disease when remissions no longer occur (3–5).

Corresponding author: Stella Elkabes, Neurology and Neuroscience, NJMS/UMDNJ, 185 South Orange Ave, MSB H-506, Newark, NJ 07103., elkabest@umdnj.edu.

[1]These two authors contributed equally to the manuscript.

Moreover, magnetic resonance imaging studies indicate abnormal structural and biochemical changes in the gray matter of MS patients as compared with healthy individuals raising the possibility of neuronal pathology or loss (6,7). However, the molecular mechanisms underlying axonal and neuronal dysfunction remain undefined.

Our previous investigations had indicated a significant decrease in neuronal PMCA2 levels at the onset of symptoms during both myelin basic protein (MBP)-induced acute EAE in the Lewis rat and myelin oligodendrocyte glycoprotein (MOG)-induced chronic EAE in the C57Bl/6 mouse, suggesting abnormalities in calcium extrusion mechanisms in the spinal cord (8,9). Moreover, a decrease in transcript levels of PMCA isoforms in postmortem MS brains has been reported (10). However, it was not yet clear whether these changes were the cause or the consequence of neuronal/axonal damage observed in these diseases. The present studies were undertaken to determine whether suppression of PMCA activity or expression causes neuronal pathology and loss, in vitro and in vivo.

Ion dyshomeostasis, and particularly perturbations in calcium balance, have received attention as major causes of axonal damage and neuronal dysfunction in many pathological conditions (11–13). Neuronal calcium influx through voltage-gated calcium channels is followed by activation of extrusion, sequestration, and buffering mechanisms, which ensure maintenance of calcium homeostasis. Extrusion of calcium from neurons is mediated by PMCAs and the Na^+/Ca^{2+} exchanger, whereas sequestration into the endoplasmic reticulum involves sarco (endo)plasmic reticulum Ca^{2+} ATPases (SERCA). In addition, mitochondria play an important role in maintaining calcium balance within the cell. The malfunction of any of these processes can elevate intracellular calcium to abnormal levels, which, in turn, can initiate injury mechanisms, including release of mitochondrial cytochrome C which activates the caspase cascade that mediates apoptotic cell death (14). A decrease in extrusion activity and the subsequent calcium overload may lead to massive calcium influx into mitochondria, resulting in the production of reactive oxygen intermediates and perturbations in energy metabolism, which may have deleterious consequences on neurons (15).

Recent studies on MS and EAE have shown an accumulation of a pore-forming subunit of N-type voltage-gated calcium channels along demyelinated, dystrophic axons, suggesting that increased calcium influx may be a cause of axonal injury (16). However, it is not known whether and how perturbations in PMCA-mediated calcium extrusion contribute to neuronal/axonal pathology.

PMCAs are P-type ATPases that play a major role in expelling calcium from cells. Four isoforms, PMCA1-4, encoded by different genes, have been described (17). The cellular and tissue distribution of these isoforms suggest that they may play distinct roles (18–21). In particular, PMCA2 and 3 are mainly localized to neurons (8,22). Moreover, the phenotype of both PMCA2-deficient mice and *deafwaddler*^{2J} (*dfw*^{2J}), a mouse with a functionally null mutation in the PMCA2 gene, indicates that this isoform plays unique roles that are not fully compensated by the presence of other isoforms (23–25). PMCA2-deficient and *dfw*^{2J} mice exhibit abnormal gait and balance, as well as hearing deficits (23,25).

Our current investigations indicate that inhibition of PMCA activity, in vitro, causes neuronal pathology followed by neuronal loss. Importantly, we report a decrease in the number of spinal cord motor neurons both in PMCA2-deficient and *dfw*^{2J} mice as compared with their wild-type controls. Therefore, our previous findings demonstrating a decrease in neuronal PMCA2 levels at onset of symptoms in animal models of MS taken together with the results reported in the present study raise the possibility that a reduction in PMCA2 expression/activity may be a cause underlying neuronal injury in EAE and potentially MS (8,9).

MATERIALS AND METHODS

Animals

Adult *dfw*^{2J} and wild-type mice were purchased from Jackson Laboratories (Bar Harbor, ME). The *dfw*^{2J} allele has evolved spontaneously in Cby.A/J-fsn, a congenic substrain of BALB/cByJ mice. PMCA2 (−/−) and (+/+) mice are a Black Swiss strain (23). All experiments were performed according to Institutional Animal Care and Use Committee guidelines.

Spinal cord neuronal cultures

Spinal cords, dissected from 15-day-old rat embryos (Charles River, Wilmington, MA) were dissociated by trituration, layered onto a 4% BSA gradient and centrifuged at 700 × *g* for 2 min. The cells were resuspended in L-15 medium containing supplements (26) and plated on poly-l-ornithine coated dishes at a density of 0.8×10^6 cells/35 mm petri dish. One day after plating, the media were replaced with Neurobasal medium supplemented with B-27, 6.3 mg/ml NaCl, and 10 U/ml penicillin/streptomycin. The cells were maintained in vitro for 8 days, until neuronal differentiation. The purity of the cultures (96–98%) was assessed by determining the percentage of NeuN (1:1000, Chemicon, Temecula, CA) and GFAP (1:10000, Dako, Carpinteria, CA) immunoreactive cells. Media and B-27 were purchased from Gibco (Rockville, MD). Other chemicals were obtained from Sigma (St. Louis, MO).

PMCA and SERCA inhibitors

5-(and-6)-carboxyeosin diacetate, succinimidyl ester (CE, Molecular Probes, Eugene, OR), thapsigargin and cyclopiazonic acid, *Penicillium cyclopium* (CPA, Calbiochem, San Diego, CA), were dissolved in DMSO. Sodium orthovanadate (Na_3VO_4, Sigma) was dissolved according to manufacturer's instructions.

MTT assay

Viability of neurons was assessed by use of 3-(4,5-dimethylthiazol-2-yl)-2,5-diphenyltetrazolium bromide (MTT, Sigma) assay (27). Cells in 15 fields were counted with a 40× objective using an Olympus IX50 microscope.

RT-PCR

RT-PCR was performed as described before (8). Briefly, DNase- treated total RNA (1–2 μg) was reverse-transcribed in a total volume of 20 μl using the Retroscript Reverse Transcription kit (Ambion, Austin, TX), according to manufacturer's instructions. Five microliters of RT mix was used for PCR in a total volume of 50 μl. PCR conditions were as follows: denaturation at 94°C for 30 s, annealing at 55°C for 45 s, and polymerization at 68°C for 1 min followed by 10 min extension at 72°C. PCR was performed for 30 cycles. The regions selected for the design of the 5′ and 3′ primers were bases 667–690 and 1659–1681 of the PMCA2 gene (GeneBank accession number J03754), respectively. The predicted size of the RT-PCR product was 1014 bp. Products were separated on a 1.5% agarose gel containing ethidium bromide (0.5 μg/ml), and the image was captured using an Alpha digital imaging system.

Immunocytochemistry

Cultures were fixed using 4% paraformaldehyde/0.1 M PBS, pH 7.5. Cells were blocked with 30% horse or goat serum/0.025–0.1% triton X-100/PBS for 1 h and incubated overnight with SMI-32 (1:3000, Sternberger Monoclonals, Lutherville, MD), antiactivated caspase-3 (1:1000, Cell Signaling, Beverly, MA) or anti-PMCA2 (1:2000, Research Diagnostics, Flanders, NJ) antibodies at 4°C. This was followed by incubation with the corresponding biotinylated secondary antibody (1:100–1:200, Vector Laboratories, Burlingame, CA) and avidin-biotin complex (Vectastain, Vector). Immunopositive cells were visualized using 3,3′-

diaminobenzidine (DAB, Sigma). Cells in 15 fields were counted using a 40× objective in an Olympus IX50 microscope. The results were analyzed by ANOVA using Scheffe's post hoc analysis or by *t* test.

Mice (3–4 mice/group) were perfused with 0.9% saline followed by 4% paraformaldehyde/0.1 M phosphate buffer, pH 7.5. The spinal cords were dissected, post-fixed, and cryoprotected. Ten-micrometer cryostat sections obtained from the lumbar spinal cord of PMCA2 (+/+) and (−/−) mice (or *dfw*^{2J} and wild-type control) were mounted on slides, side by side. The beginning of the lumbar enlargement at the L1 level was used as a landmark for the first section obtained from spinal cords. Seven to ten sections, collected from each lumbar spinal cord at 100-μm intervals, were used for immunocytochemistry. This ensured that each cell was counted only once. In addition, adjacent sections were stained with cresyl violet, and the outline of the gray matter was analyzed under the microscope to further ascertain that the sections derived from control and experimental specimens represented comparable levels of the lumbar spinal cord. Immunocytochemistry was performed as described above using antiperipherin (1:4000, Chemicon) or SMI-32 (1:6000) antibodies. Negative controls, treated in the same manner except incubation with primary antibody, did not produce any signal. Because SMI-32, a monoclonal antibody, was used to label mouse tissue, the specificity of the signal was assessed employing the Mouse Over Mouse (MOM) kit (Vector) according to the manufacturer's instructions. The signals obtained with MOM and the method described above were identical. Immunoreactive cells were counted with a 20× objective employing an Olympus BX41 microscope.

The gray matter area was quantified by use of a Nikon Microphot AF microscope with a Kodak Spot III digital camera and Ph3 Imaging (Ph3, Inc., Philadelphia, PA) software. Number of cells/mm^2 was calculated by dividing the total number of immunoreactive cells in each section by the gray matter area of the same section.

Quantification of intracellular calcium levels

Spinal cord cells, cultured for 8 days on poly-l-ornithine coated glass cover slips, were loaded with 4 μM Fura-2/acetoxymethyl ester (Molecular Probes) in medium for 30 min and washed with medium C for 30 min at 37°C. The medium was then replaced with 360 μl recording buffer (8 mM Na_2HPO_4, 1.5 mM $KHPO_4$, 138 mM NaCl, 2.7 mM KCl, 20 mM HEPES, 1.3 mM $CaCl_2$, 0.8 mM $MgCl_2$, 5 mM glucose). Cover slips were mounted onto a 37°C recording chamber installed on the stage of an inverted microscope (Nikon Diaphot 300, Japan). Cells were incubated with CE or vehicle (0.1% DMSO) during Fura-2 loading and subsequent steps. The concentration of CE used (5–20 μM) does not inhibit other Ca^{2+} ATPases (28). For Fura-2 dual excitation, the beam of light from a high-pressure xenon bulb set was passed through a 340/380 nm shutter/filter wheel (Applied Imaging, Visitech Int., UK) at 0.2 Hz. The emitted fluorescence was collected by a 40× oil objective and detected at 510 nm. Fluorescence signals were digitized and stored on disk using Quanticell 700 (Applied Imaging). Cells were depolarized by applying 40 μl of high K^+ solution (100 mM KCl, 8 mM Na_2HPO_4, 1.5 mM $KHPO_4$, 38 mM NaCl, 2.7 mM KCl, 20 mM HEPES, 1.3 mM $CaCl_2$, 0.8 mM $MgCl_2$, 5 mM glucose) at t = 46–49 s, and responses were recorded for additional 750 s. Free intracellular calcium concentration ($[Ca^{2+}]i$) was monitored by using Fura-2 ratio imaging with the parameters: $R = F340/F380$, $R\text{min} = 0.3$, $R\text{max} = 3$, $\beta = 3.42$ and $KD = 220$ nM (29). Differences in calcium levels before KCl (basal) at KCl-induced peak, 350 s after KCl (t = 400 s) and at endpoint (t = 800 s) were analyzed using ANOVA for repeated measures with one between subject factor (CE treatment) and one within subject factor (time) followed by Tukey's post hoc test. The clearance rates (t1/2 and t1/3) were obtained from each trace. When the clearance rate was superior to recording time (800–830 s), it was cut off at 800 s for statistical analysis.

Differences between groups were analyzed using factorial ANOVA followed by Tukey's post hoc test.

RESULTS

Blockade of PMCA activity induces neuronal pathology and death

To investigate the effects of calcium pump inhibitors on neuronal function, we employed purified spinal cord neuronal cultures, which were maintained in vitro for eight days. We first ascertained that PMCA2 mRNA and protein were expressed in these cultures. RT-PCR amplified a band of the expected size (8, Fig. 1A). The identity of this band was further confirmed by sequence analysis. PMCA2 protein was also detected in cell bodies and processes by immunocytochemistry using an antibody specific for this pump (Fig. 1*B*).

Initially, we exposed cells to different concentrations of Na_3VO_4, a general inhibitor of P-type ATPases, including PMCAs and SERCA pumps (30–32). Subsequently, we assessed immunoreactivity to nonphosphorylated neurofilament H by use of the SMI-32 antibody, a marker of neuronal/axonal damage in MS, EAE, and other pathological conditions of the CNS (33–35). Thirty μM Na_3VO_4, an optimal dose, significantly increased the number of SMI-32 positive cells within 4 h (Fig. 1*C*). A lower dose (10 μM) was also effective when cells were exposed to the inhibitor for 8 h. Since Na_3VO_4 can also interfere with the activity of SERCA pumps, we investigated whether cyclopiazonic acid (10 μM) and thapsigargin (250 nM), specific SERCA pump inhibitors, induce a similar response (36,37). The doses employed were maximally effective as reported previously (36) and as indicated by our preliminary experiments. We did not observe any significant changes in the SMI-32 positive cell number (Fig. 1*D*). These results suggested that Na_3VO_4-induced neuronal pathology might primarily be due to inhibition of PMCAs.

To further ascertain that the changes in SMI-32 immunopositive neuron number were indeed due to blockade of PMCA activity, we employed 5-(and-6)-carboxyeosin (CE), a more selective and potent PMCA inhibitor (38–40). Cultures were treated with medium/vehicle or 5 μM CE (optimal dose, range tested 0–20 μM) for 2, 4, and 8 h. Exposure to CE for 4 h induced a 1.8-fold increase in SMI-32 positive cells (Fig. 1*E*). The diverse morphology of these cells suggested that different neuronal subpopulations were affected. Surprisingly, SMI-32 positive cell number in CE-treated cultures was not significantly different from controls at 8 h. One potential interpretation of these findings was that exposure of cultures to CE for 4 h increases immunoreactivity to nonphosphorylated neurofilament H, which is then followed by loss of SMI-32 positive affected cells at 8 h. To test this possibility, we investigated cell survival by use of MTT assay. Indeed, a reduction in MTT-positive cells was observed by 8 h (Fig. 1*F*). Thus, prolonged exposure to CE affects neuronal survival.

Inhibition of PMCA activity and the resulting aberrance in calcium extrusion may lead to abnormal increases in intracellular calcium levels ($[Ca^{2+}]i$), which promote mitochondrial cytochrome C release, a trigger that activates the caspase cascade mediating apoptotic cell death (41). To determine whether blockade of PMCA activity induces apoptotic mechanisms, we quantified the number of cells expressing activated caspase-3, a key component of apoptosis. There was a twofold increase in the number of caspase-3 positive cells in cultures treated with CE for 8 h suggesting that cell death may partially be due to apoptosis (Fig. 1*G*). Thus, our results indicate that CE-induced neuronal damage, detected initially by changes in neurite morphology and increased SMI-32 immunoreactivity, is followed by activation of caspase-3 and neuronal loss.

It is worth noting that although extended exposure to Na_3VO_4 increased SMI-32 positive cell number, the inhibitor did not induce neuronal death within the period employed in the present

investigation. The difference in the actions of Na_3VO_4 and CE may be due to the limited penetration of Na_3VO_4 into intact cells, higher selectivity and potency of CE, or different modes of interaction of the two inhibitors with PMCAs (30,38).

The results reported above reflected the overall effects of CE on multiple spinal cord neuronal populations present in our cultures. Because motor neurons constitute only 2–4% of the total neurons in the dish and are known to be most vulnerable to calcium-mediated injury, we next studied the effects of CE on this neuronal subpopulation. Motor neurons were identified by their distinctive morphology, which includes a very large cell body, a long axon and multiple dendrites. Quantification in controls and CE treated cultures indicated a 45% decrease in the number of cells exhibiting motor-neuron like morphology in cultures treated with CE for 4 h as compared with controls (Control: 99.5±9.9%; CE: 55.2± 5.2%, values are expressed as percent control, $P < 0.007$ by Student's *t* test). A further decrease was observed eight hours after addition of CE (Control: 101.5±6.9%; CE: 31±5.5%; values are expressed as percent control, $P < 0.0002$ by *t* test). Thus, the loss of motor neuron-like cells at 4 hours, prior to the death of some other neuronal populations found in our cultures, indicates that these cells are particularly vulnerable to alterations in PMCA-mediated calcium extrusion.

Inhibition of PMCA activity induces morphological abnormalities in neuritic processes

In addition to the increase in SMI-32-positive cell number described above, treatment of spinal cord neuronal cultures with CE for 4 h also affected the morphology of neurites (Fig. 2). In control cultures, maintained only in medium and vehicle, a small subpopulation of cells constituting ~2–4% of the total cells in the dish, was immunopositive for SMI-32 (Fig. 2*A*). These cells exhibited motor neuron-like morphology and had long, smooth and SMI-32-positive processes. Indeed, previous studies reported SMI-32 immunoreactivity in cultured motor neurons, even in the absence of a pathological challenge (42). Addition of 5 μM CE to sister cultures initiated swelling and beading of neurites within 2 h (data not shown), which became further pronounced after 4 h (Fig. 2*B* and *C*). This morphology contrasted with the smooth appearance of the majority of SMI-32 positive processes in control cultures (Fig. 2*D*). Whereas in controls only 10.2 ± 2.63% of all SMI-32-positive cells showed occasional swellings in their processes, in CE treated cultures, 42.4 ± 2.39% of SMI-32-positive cells had neurites with frequent beading and swellings ($P < 0.0001$ by Student's *t* test). In addition, spherical structures, reminiscent of axonal retraction bulbs, could be observed at the end of many processes (Fig. 2*E*). Disintegration of some neurites occurred at 8 h and paralleled cell death (not shown).

Inhibition of PMCA activity delays recovery from depolarization-evoked increases in intracellular calcium

Because PMCAs play a major role in calcium extrusion, we hypothesized that a decrease in PMCA activity may lead to alterations in $[Ca^{2+}]i$, which, in turn, induces injury cascades. To determine the effects of CE on intracellular calcium balance in spinal cord neurons, cultures were incubated with either vehicle or 5 and 20 μM CE for only 1 h, a time that precedes the appearance of morphological changes in neurites. This treatment elevated the resting cytosolic calcium levels by 27 nM and 81 nM when 5 μM CE and 20 μM CE were used, respectively (Fig. 3*A* and *B*). Moreover, the clearance of depolarization-induced Ca^{2+} transients was significantly slower in CE-treated cells than controls (Fig. 3). The rate of Ca^{2+} clearance was estimated by analyzing the time for half (t1/2) and one third (t1/3) decay of the $[Ca^{2+}]i$ transients induced by high K^+ buffer. Calcium clearance was at least fivefold slower in CE-treated groups as compared with controls. Strikingly, 9% of the cells exposed to 5 μM CE and 55% of the cells treated with 20 μM CE exhibited a very slow calcium clearance rate (t1/2 > 800 s), while the remaining cells had t1/2 values of 294±15 and 196±17 s, respectively. This suggests that one or more neuronal subpopulations may be extremely dependent on PMCA activity for

calcium removal. The amplitudes of depolarization-induced $[Ca^{2+}]i$ peaks were also greatly increased in the presence of CE, in a dose-dependent manner.

These results indicate that PMCA activity is critical for the maintenance of resting $[Ca^{2+}]i$ and for recovery from K^+ induced $[Ca^{2+}]i$ rise in spinal cord neurons. Moreover, our findings suggest that approximately half of the cells in our cultures are highly dependent on PMCA activity for recovery from depolarization-evoked calcium transients.

Loss of motor neurons in the spinal cord of PMCA2 null mice and *dfw^{2J}* mutant mice

To determine whether the lack of PMCA2 causes neuronal loss, in vivo, we quantified the number of SMI-32 positive cells in spinal cord sections of PMCA2 (+/+) and (−/−) mice. In particular, we focused on motor neurons, because they are highly vulnerable to changes in intracellular calcium levels and Ca^{2+}-mediated injury (42). Staining for SMI-32, a marker for motor neurons (42), was confined to somata of anterior horn cells exhibiting the characteristic, motor neuron-like morphology both in wild-type and knockout mice. There was a 37.5% decrease in the number of SMI-32-positive cells in PMCA2-deficient mice as compared with their wild-type littermates (Fig. 4*A*). We also analyzed the results by calculating the SMI-32 positive cell number/mm^2 gray matter (Fig. 4*B*), as the total gray matter area is 13% smaller in PMCA2 (−/−) as compared with PMCA2 (+/+) mice (Fig. 4*C*). There was a 26.5% decrease in SMI-32 immunoreactive cells/mm^2 gray matter in PMCA2 knockout mice as compared with wild-type controls.

To corroborate these findings, we labeled adjacent sections with an antibody against peripherin, another marker for motor neurons (42). Peripherin immunoreactivity was strongest in anterior horn cells with motor neuron-like morphology but could also be observed, to a lesser extent and intensity, in some smaller cells of the gray matter. In agreement with the results obtained by use of SMI-32, we found a significant decrease in the number of peripherin immunoreactive cells and peripherin-positive cells/mm^2 gray matter (37.4 and 27.7%, respectively) in PMCA2 (−/−) as compared with PMCA2 (+/+) mice (Fig. 4*D*–4*G*).

To further ensure that the lack of PMCA2 activity decreases the number of motor neurons, we quantified SMI-32 positive cells in the spinal cord of *dfw^{2J}* mice. A two base-pair deletion in the PMCA2 gene of *dfw^{2J}* causes a frameshift leading to a truncated, inactive protein (25). In agreement with the studies on PMCA2 (−/−) mice, we found a 41% decrease in the number of SMI-32-positive cells in *dfw^{2J}* mice as compared with their wild-type controls (Fig. 5*A*). We also found a 39% decrease in SMI-32-positive cell number/mm^2 gray matter (Fig. 5*B*) when the small but significant 12% decrease in gray matter area of the *dfw^{2J}* spinal cord was taken into consideration (Fig. 5*C*).

These results, taken together, indicate that the lack of PMCA2 expression in PMCA2 (−/−) mice or a functionally null mutation in the PMCA2 gene in *dfw^{2J}*, have similar effects resulting in a decrease in the number of SMI-32 positive motor neuron-like cells in the spinal cord. It is worth noting that our results do not exclude the possibility that additional neuronal subpopulations may also be affected in the spinal cord of PMCA2-deficient and mutant mice.

DISCUSSION

Axonal damage and neuronal loss occur in many CNS disorders, including MS and spinal cord injury. Yet, the triggers that initiate axonal pathology, the underlying mechanisms, and the critical molecules, which may be targets for therapeutic interventions, are not well defined. Our present findings indicate that inhibition of PMCA activity in neuronal cultures, delays calcium clearance, induces cytoskeletal abnormalities, promotes swelling of neurites and finally causes neuronal death. Reductions in PMCA levels and/or activity may first induce

intracellular calcium overload due to delayed clearance resulting from abnormalities in extrusion mechanisms. Subsequently, elevated calcium can cause changes in cytoskeletal proteins as suggested by increased nonphosphorylated neurofilament H (SMI-32)-positive cell number and alterations in SMI-32 immunoreactive neurite morphology. The changes in neurite morphology appear to be similar to those observed after addition of the calcium ionophore A23187 to spinal cord neuronal cultures, which promotes beading, disruption of the cytoskeleton, and mitochondrial abnormalities (43). As changes in cytoskeletal proteins may interfere with axonal transport, swellings may be the consequence of the accumulation of organelles, cytoplasm, and fragmented neurofilaments in affected processes. Furthermore, PMCAs are localized to both synaptic terminals and dendrites (21). Thus, a reduction in PMCA activity may damage not only axons but also dendrites, which are affected during EAE (44). Indeed, it has been suggested that dendritic arborization of Purkinje cells in PMCA2 null mice is reduced as compared with their wild-type littermates (23). Such changes may alter synaptic function and neuronal communication as well as survival. In fact, the early pathological changes observed in our neuronal cultures are followed by activation of death pathways, including apoptotic mechanisms, resulting in neuronal loss as indicated by an increase in activated caspase-3 positive cells and a reduction in MTT positive cells. The decrease in SMI-32 and peripherin immunoreactive neuron number in PMCA2-deficient mice and the reduction in SMI-32 positive cell number in *dfw*^{2J} mice as compared with their respective wild-type controls further support this notion. Thus, a perturbation in PMCA-mediated calcium extrusion may be an important contributor to axonal and neuronal damage in pathological conditions of the CNS, including EAE, MS, and spinal cord injury. Importantly, our previous results indicate a decline in the levels of PMCA2 in two different animal models of MS with distinct disease course and histopathological characteristics (8,9). This finding is of particular significance as axonal pathology and neuronal loss has been reported in both models and suggests similarities in molecular mechanisms underlying neuronal damage during acute and chronic EAE (34,35).

It is worth noting that the findings of the present study may also be relevant to other pathological conditions of the CNS, including spinal cord trauma, as we and others have reported a decrease in PMCA2 transcript levels after spinal cord contusion injury (45,46). It is possible that anomalies in PMCA-mediated calcium extrusion contribute to secondary neuronal/axonal damage after spinal cord injury, expanding the deleterious effects of the first traumatic impact. Calcium has also been implicated in the degeneration of axons in the white matter after anoxia/ischemia (47). It has been hypothesized that the energy depletion following hypoxia or ischemia results in failure of Na^+/K^+ ATPase and activation of sodium channels, which augments axoplasmic Na^+ concentrations. This, in turn, causes the reversal of Na^+/Ca^{2+} exchanger (NCX) activity, thus increasing calcium levels (48). Moreover, calcium influx through sodium channels further augments axoplasmic calcium concentrations (12). As a consequence, protease-mediated injury cascades are activated (49). In agreement with these results, blockade of sodium channels and NCX prevents axonal deterioration in anoxia (50,51). Interestingly, similar mechanisms have recently been implicated in MS and EAE (52,53). In addition, recent studies have suggested that ryanodine receptor-mediated release of calcium from the endoplasmic reticulum causes abnormal elevations in calcium concentrations within the axoplasm promoting injury during spinal cord ischemia (54).

In summary, our findings and those reported by others indicate that axonal and neuronal pathology in CNS disorders and trauma may be governed by multiple mechanisms. Modifications in the function of calcium channels, NCX, and PMCA may all contribute to the disruption of calcium balance, a key element playing a pivotal role in cellular pathology and death. These findings also raise the possibility that independent of the initial trigger inducing neuronal/axonal damage, the molecular mechanisms underlying neuronal injury in different pathological conditions of the CNS may share commonalties.

Acknowledgments

This work was supported by grants 01-3008-SCR-S-0 from NJCSCR and NS 046363 from NIH/NINDS to SE; HL61974 from NIH/NHLBI to GES and INSERM funds to AN. We thank the Kirby Foundation (SE) for the support of this work. We are grateful to Dr. C. Collet for assistance in calcium imaging and analysis and Dr. P. Kitabgi for his support of this work.

References

1. Zamvil SS, Steinman L. Diverse targets for intervention during inflammatory and neurodegenerative phases of multiple sclerosis. Neuron 2003;38:685–688. [PubMed: 12797954]
2. Hickey WF. The pathology of multiple sclerosis: a historical perspective. J Neuroimmunol 1999;98:37–44. [PubMed: 10426360]
3. Ferguson B, Matyszak MK, Esiri MM, Perry VH. Axonal damage in acute multiple sclerosis lesions. Brain 1997;120:393–399. [PubMed: 9126051]
4. Trapp BD, Peterson J, Ransohoff RM, Rudick R, Mork S, Bo L. Axonal transection in the lesions of multiple sclerosis. N Engl J Med 1998;338:278–285. [PubMed: 9445407]
5. Filippi M, Bozzali M, Rovaris M, Gonen O, Kesavadas C, Ghezzi A, Martinelli V, Grossman RI, Scotti G, Comi G, et al. Evidence for widespread axonal damage at the earliest clinical stage of multiple sclerosis. Brain 2003;126:433–437. [PubMed: 12538409]
6. Ge Y, Grossman RI, Udupa JK, Babb JS, Kolson DL, McGowan JC. Magnetization transfer ratio histogram analysis of gray matter in relapsing-remitting multiple sclerosis. AJNR Am J Neuroradiol 2001;22:470–475. [PubMed: 11237968]
7. Bozzali M, Cercignani M, Sormani MP, Comi G, Filippi M. Quantification of brain gray matter damage in different MS phenotypes by use of diffusion tensor MR imaging. AJNR Am J Neuroradiol 2002;23:985–988. [PubMed: 12063230]
8. Nicot A, Ratnakar PV, Ron Y, Chen CC, Elkabes S. Regulation of gene expression in experimental autoimmune encephalomyelitis indicates early neuronal dysfunction. Brain 2003;126:398–412. [PubMed: 12538406]
9. Nicot A, Kurnellas M, Elkabes S. Temporal expression of plasma membrane calcium ATPases in the spinal cord during the clinical course of experimental autoimmune encephalomyelitis. J Neurol 2003;250(Suppl 2):143.
10. Lock C, Hermans G, Pedotti R, Brendolan A, Schadt E, Garren H, Langer-Gould A, Strober S, Cannella B, Allard J, et al. Gene-microarray analysis of multiple sclerosis lesions yields new targets validated in autoimmune encephalomyelitis. Nat Med 2002;8:500–508. [PubMed: 11984595]
11. LoPachin RM, Lehning EJ. Mechanism of calcium entry during axon injury and degeneration. Toxicol Appl Pharmacol 1997;143:233–244. [PubMed: 9144441]
12. Wolf JA, Stys PK, Lusardi T, Meaney D, Smith DH. Traumatic axonal injury induces calcium influx modulated by tetrodotoxin-sensitive sodium channels. J Neurosci 2001;21:1923–1930. [PubMed: 11245677]
13. Kapoor R, Davies M, Blaker PA, Hall SM, Smith KJ. Blockers of sodium and calcium entry protect axons from nitric oxide-mediated degeneration. Ann Neurol 2003;53:174–180. [PubMed: 12557283]
14. Tymianski M, Tator CH. Normal and abnormal calcium homeostasis in neurons: a basis for the pathophysiology of traumatic and ischemic central nervous system injury. Neurosurgery 1996;38:1176–1195. [PubMed: 8727150]
15. Paschen W. Role of calcium in neuronal cell injury: which subcellular compartment is involved? Brain Res Bull 2000;53:409–413. [PubMed: 11136996]
16. Kornek B, Storch MK, Bauer J, Djamshidian A, Weissert R, Wallstroem E, Stefferl A, Zimprich F, Olsson T, Linington C, et al. Distribution of a calcium channel subunit in dystrophic axons in multiple sclerosis and experimental autoimmune encephalomyelitis. Brain 2001;124:1114–1124. [PubMed: 11353727]
17. Strehler EE, Zacharias DA. Role of alternative splicing in generating isoform diversity among plasma membrane calcium pumps. Physiol Rev 2001;81:21–50. [PubMed: 11152753]

18. Filoteo AG, Elwess NL, Enyedi A, Caride A, Aung HH, Penniston JT. Plasma membrane Ca^{2+} pump in rat brain. Patterns of alternative splices seen by isoform-specific antibodies. J Biol Chem 1997;272:23,741–23,747.
19. Stauffer TP, Guerini D, Celio MR, Carafoli E. Immunolocalization of the plasma membrane Ca^{2+} pump isoforms in the rat brain. Brain Res 1997;748:21–29. [PubMed: 9067441]
20. Lehotsky J, Kaplan P, Murin R, Raeymaekers L. The role of plasma membrane Ca2+ pumps (PMCAs) in pathologies of mammalian cells. Front Biosci 2002;7:D53–D84. [PubMed: 11779702]
21. Burette A, Rockwood JM, Strehler EE, Weinberg RJ. Isoform-specific distribution of the plasma membrane Ca^{2+} ATPase in the rat brain. J Comp Neurol 2003;467:464–476. [PubMed: 14624481]
22. Garcia ML, Strehler EE. Plasma membrane calcium ATPases as critical regulators of calcium homeostasis during neuronal cell function. Front Biosci 1999;4:D869–D882. [PubMed: 10577388]
23. Kozel PJ, Friedman RA, Erway LC, Yamoah EN, Liu LH, Riddle T, Duffy JJ, Doetschman T, Miller ML, Cardell EL, et al. Balance and hearing deficits in mice with a null mutation in the gene encoding plasma membrane Ca^{2+}-ATPase isoform 2. J Biol Chem 1998;273:18,693–18,696.
24. Shull GE. Gene knockout studies of Ca^{2+}-transporting ATPases. Eur J Biochem 2000;267:5284–5290. [PubMed: 10951186]
25. Street VA, McKee-Johnson JW, Fonseca RC, Tempel BL, Noben-Trauth K. Mutations in a plasma membrane Ca^{2+}-ATPase gene cause deafness in deafwaddler mice. Nat Genet 1998;19:390–394. [PubMed: 9697703]
26. Camu W, Henderson CE. Purification of embryonic rat motoneurons by panning on a monoclonal antibody to the low-affinity NGF receptor. J Neurosci Methods 1992;44:59–70. [PubMed: 1434751]
27. Mosmann T. Rapid colorimetric assay for cellular growth and survival: application to proliferation and cytotoxicity assays. J Immunol Methods 1983;65:55–63. [PubMed: 6606682]
28. Gatto C, Hale CC, Xu W, Milanick MA. Eosin, a potent inhibitor of the plasma membrane Ca pump, does not inhibit the cardiac Na^{+}-Ca^{2+} exchanger. Biochemistry 1995;34:965–972. [PubMed: 7530047]
29. Grynkiewicz G, Poenie M, Tsien RY. A new generation of Ca^{2+} indicators with greatly improved fluorescence properties. J Biol Chem 1985;260:3440–3450. [PubMed: 3838314]
30. Barrabin H, Garrahan PJ, Rega AF. Vanadate inhibition of the Ca^{2+}-ATPase from human red cell membranes. Biochim Biophys Acta 1980;600:796–804. [PubMed: 6447514]
31. Tiffert T, Lew VL. Kinetics of inhibition of the plasma membrane calcium pump by vanadate in intact human red cells. Cell Calcium 2001;30:337–342. [PubMed: 11733940]
32. De Luisi A, Hofer AM. Evidence that Ca(2+) cycling by the plasma membrane Ca(2+)-ATPase increases the 'excitability' of the extracellular Ca(2+)-sensing receptor. J Cell Sci 2003;116:1527–1538. [PubMed: 12640037]
33. Leifer D, Kowall NW. Immunohistochemical patterns of selective cellular vulnerability in human cerebral ischemia. J Neurol Sci 1993;119:217–228. [PubMed: 8277338]
34. Pitt D, Werner P, Raine CS. Glutamate excitotoxicity in a model of multiple sclerosis. Nat Med 2000;6:67–70. [PubMed: 10613826]
35. Smith T, Groom A, Zhu B, Turski L. Autoimmune encephalomyelitis ameliorated by AMPA antagonists. Nat Med 2000;6:62–66. [PubMed: 10613825]
36. Scamps F, Vigues S, Restituito S, Campo B, Roig A, Charnet P, Valmier J. Sarco-endoplasmic ATPase blocker 2,5-Di(tert-butyl)-1, 4-benzohydroquinone inhibits N-, P-, and Q- but not T-, L-, or R-type calcium currents in central and peripheral neurons. Mol Pharmacol 2000;58:18–26. [PubMed: 10860923]
37. Bardo S, Robertson B, Stephens GJ. Presynaptic internal Ca^{2+} stores contribute to inhibitory neurotransmitter release onto mouse cerebellar Purkinje cells. Br J Pharmacol 2002;137:529–537. [PubMed: 12359635]
38. Gatto C, Milanick MA. Inhibition of the red blood cell calcium pump by eosin and other fluorescein analogues. Am J Physiol 1993;264:C1577–C1586. [PubMed: 7687411]
39. Fierro L, DiPolo R, Llano I. Intracellular calcium clearance in Purkinje cell somata from rat cerebellar slices. J Physiol 1998;510:499–512. [PubMed: 9705999]

40. Sedova M, Blatter LA. Dynamic regulation of [Ca2+]i by plasma membrane Ca(2+)-ATPase and Na+/Ca2+ exchange during capacitative Ca2+ entry in bovine vascular endothelial cells. Cell Calcium 1999;25:333–343. [PubMed: 10463097]
41. Budihardjo I, Oliver H, Lutter M, Luo X, Wang X. Biochemical pathways of caspase activation during apoptosis. Annu Rev Cell Dev Biol 1999;15:269–290. [PubMed: 10611963]
42. Carriedo SG, Yin HZ, Lamberta R, Weiss JH. In vitro kainate injury to large, SMI-32(+) spinal neurons is Ca^{2+} dependent. Neuroreport 1995;6:945–948. [PubMed: 7612889]
43. Emery DG, Lucas JH. Ultrastructural damage and neuritic beading in cold-stressed spinal neurons with comparisons to NMDA and A23187 toxicity. Brain Res 1995;692:161–173. [PubMed: 8548300]
44. Zhu B, Luo L, Moore GR, Paty DW, Cynader MS. Dendritic and synaptic pathology in experimental autoimmune encephalomyelitis. Am J Pathol 2003;162:1639–1650. [PubMed: 12707048]
45. Carmel JB, Galante A, Soteropoulos P, Tolias P, Recce M, Young W, Hart RP. Gene expression profiling of acute spinal cord injury reveals spreading inflammatory signals and neuron loss. Physiol Genomics 2001;7:201–213. [PubMed: 11773606]
46. Elkabes S, Nicot A. Aberrant calcium extrusion mechanisms may contribute to secondary spinal cord injury. J Neurol 2003;250(suppl 2):179. [PubMed: 12574948]
47. Stys PK, Waxman SG, Ransom BR. Ionic mechanisms of anoxic injury in mammalian CNS white matter: role of Na+ channels and Na(+)-Ca^{2+} exchanger. J Neurosci 1992;12:430–439. [PubMed: 1311030]
48. Lehning EJ, Doshi R, Isaksson N, Stys PK, LoPachin RM Jr. Mechanisms of injury-induced calcium entry into peripheral nerve myelinated axons: role of reverse sodium-calcium exchange. J Neurochem 1996;66:493–500. [PubMed: 8592118]
49. Stys PK, Jiang Q. Calpain-dependent neurofilament breakdown in anoxic and ischemic rat central axons. Neurosci Lett 2002;328:150–154. [PubMed: 12133577]
50. Fern R, Ransom BR, Stys PK, Waxman SG. Pharmacological protection of CNS white matter during anoxia: actions of phenytoin, carbamazepine and diazepam. J Pharmacol Exp Ther 1993;266:1549–1555. [PubMed: 8371157]
51. Stys PK, Lesiuk H. Correlation between electrophysiological effects of mexiletine and ischemic protection in central nervous system white matter. Neuroscience 1996;71:27–36. [PubMed: 8834390]
52. Waxman SG. Ion channels and neuronal dysfunction in multiple sclerosis. Arch Neurol 2002;59:1377–1380. [PubMed: 12223023]
53. Craner MJ, Hains BC, Lo AC, Black JA, Waxman SG. Co-localization of sodium channel Nav1.6 and the sodium-calcium exchanger at sites of axonal injury in the spinal cord in EAE. Brain 2004;127:294–303. [PubMed: 14662515]
54. Ouardouz M, Nikolaeva MA, Coderre E, Zamponi GW, McRory JE, Trapp BD, Yin X, Wang W, Woulfe J, Stys PK. Depolarization-induced Ca^{2+} release in ischemic spinal cord white matter involves L-type Ca^{2+} channel activation of ryanodine receptors. Neuron 2003;40:53–63. [PubMed: 14527433]

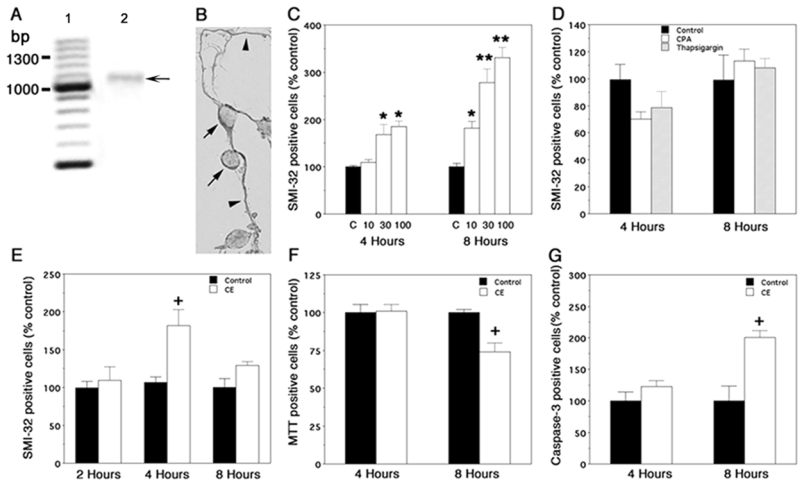

Figure 1. Effects of PMCA and SERCA inhibitors on spinal cord neurons, in vitro

A) RT-PCR showing expression of PMCA2 in neuronal cultures. Lane 1: molecular weight marker; bp, base pairs; lane 2: RT-PCR product (arrow) at the predicted molecular weight (1014 bp). The identity of the band was further verified by sequence analysis. ***B)*** PMCA2 immunoreactivity in spinal cord neurons. Arrows and arrowheads point at immunopositive cells and processes, respectively. ***C)*** SMI-32 positive cell number after exposure of cultures to 10, 30, and 100 μM Na_3VO_4. C: control. ***D)*** Effects of SERCA inhibitors on SMI-32 positive cell number. CPA: cyclopiazonic acid. ***E)*** SMI-32 positive cells after exposure of cultures to 5 μM 5-(and-6)-carboxyeosin diacetate, succinimidyl ester (CE). ***F)*** Effects of CE on cell survival. ***G)*** Induction of activated caspase-3 in cells treated with CE. The experiments were repeated at least twice and yielded similar results. Values are presented as means ± SEM. Significantly different from controls **P* < 0.003, ***P*< 0.0001 by ANOVA; +, significantly different from control by Student's *t* test, *P* < 0.02; *n* = 6–12.

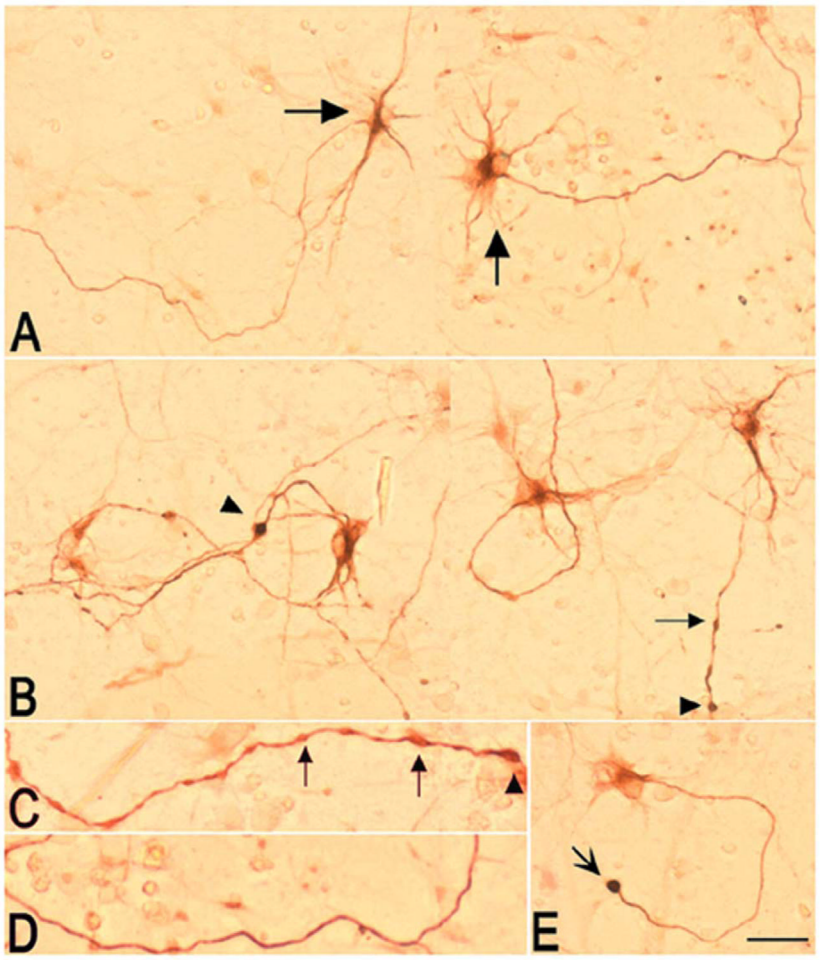

Figure 2. Effects of CE on the morphology of SMI-32 immunoreactive neurites in spinal cord neuronal cultures

A) Composite picture showing two fields of a control culture maintained in medium/vehicle. A subpopulation of cells with motor neuron-like morphology (big arrows) and their processes are SMI-32 positive as reported previously (42). ***B)*** Composite picture showing two fields of a culture treated with 5 μM CE for 4 h. Addition of CE, induced beading (small arrows) and swelling (arrowhead) of neurites. ***C)*** High magnification picture of a neurite in a CE-treated culture showing beadings (small arrows) and swellings (arrowheads). ***D)*** High magnification picture of a neurite in a control culture showing a smooth process. ***E)*** An SMI-32 positive cell in a CE-treated culture showing a spherical structure resembling a retraction bulb (concave arrow). The experiment was repeated twice and yielded similar results (n=8). Bar = 100 μm.

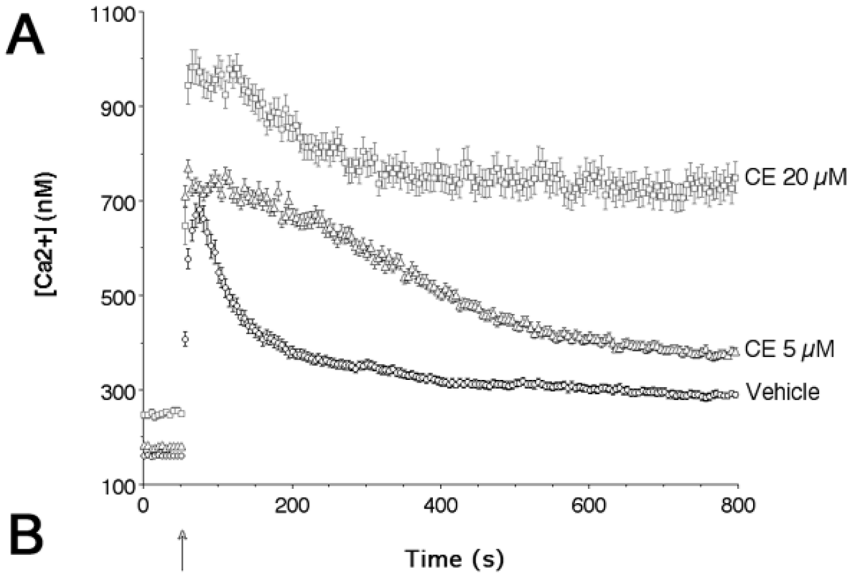

Treatment (cell #)	Calcium levels (nM) Basal	Peak	400s	End point	Clearance time (s) t1/2	t1/3
Vehicle (72)	161±3	745±33	317±8	300±10	75±5	37±3
CE 5μM (88)	175±2	858±26**	511±15**	370±11*	337±20**	191±13**
CE 20 μM (45)	240±8**	1096±4**	751±37**	751±39**	531±46**	295±42**

Figure 3. Effect of CE on basal and depolarization-evoked [Ca^{2+}]i levels in spinal cord neuronal cultures

A) [Ca^{2+}]i changes in cells loaded with Fura-2. High K^+ buffer was added at t = 46–49 s (arrow). Preincubation with CE for 1 h increased resting [Ca^{2+}]i and prolonged the recovery from depolarization-evoked Ca^{2+} transients. The amplitudes of depolarization-induced [Ca^{2+}]i peaks were also greatly increased by CE treatment. Values are presented as means ± SEM. ***B)*** Table summarizing calcium levels and clearance rates before KCl (basal), at KCl-induced peak, at 400 s (350 s after KCL addition) and at end point (t=800 s) in the experiments (***A***). t1/2 and t1/3 are half and one-third the time required to clear calcium transients, respectively. ANOVA for calcium levels: dose effect, $F_{(2,202)} = 93.3$, $P < 0.0001$; time effect, $F_{(3,606)} = 897$, $P < 0.0001$; dose X time interaction, $F_{(6,606)} = 26.4$, $P < 0.0001$; post hoc analysis: $*P < 0.05$; $**P < 0.01$ CE vs. vehicle. ANOVA for t1/3: $F_{(2,204)} = 41.4$, $P < 0.0001$; post hoc analysis: $**P < 0.01$ CE vs. vehicle. ANOVA for t1/2: $F_{(2,204)} = 85.0$, $P < 0.0001$; post hoc analysis: $**P < 0.01$ CE vs. vehicle.

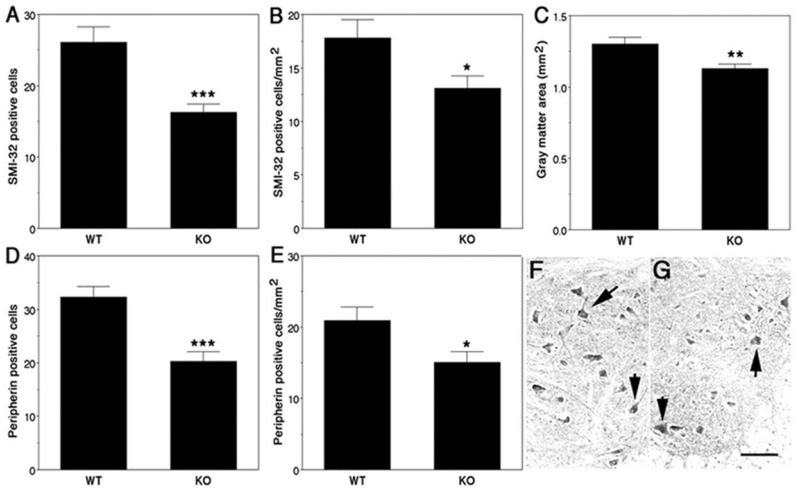

Figure 4. Loss of SMI-32 and peripherin positive neurons in the spinal cord of PMCA2 knockout (KO) mice

The number of SMI-32 positive cells/spinal cord section is decreased in KO as compared with wild-type (WT) mice (***A***). SMI-32 positive cells/mm^2 gray matter is also lower in KO mice (***B***) when the reduction in gray matter area is taken into consideration (***C***). Peripherin-positive cells/spinal cord section (***D***) and peripherin-positive cells/mm^2 gray matter (***E***) are significantly reduced in KO as compared with WT mice. Peripherin-immunoreactive motor neurons in the anterior horn of WT (***F***; arrows) and KO mouse (***G***). Four WT and KO mice were used and seven sections collected from each lumbar spinal cord at 100 μm intervals, were analyzed. Values are presented as means ± SEM. Significantly different from WT **P* < 0.03, ***P* < 0.01, ****P* < 0.0002 by Student's *t* test. Bar = 200 μm.

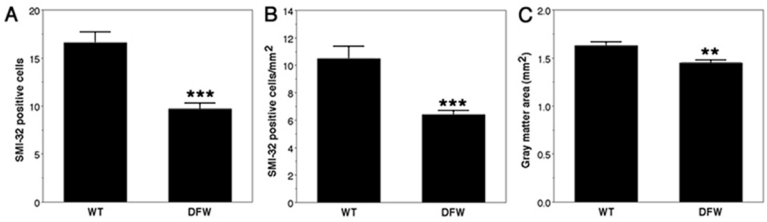

Figure 5. Loss of SMI-32 positive cells in the spinal cord of *dfw*^{2J} mice (DFW)

SMI-32 positive cells are decreased in the spinal cord of *dfw*^{2J} as compared with its wild-type (WT) control (***A***). SMI-32-positive cells/mm^2 gray matter is also lower in *dfw*^{2J} (***B***) when the reduction in gray matter area is taken into consideration (***C***). Three *dfw*^{2J} and WT mice were used. Ten sections obtained from each lumbar spinal cord at 100 μm intervals were analyzed. Values are presented as means ± SEM. Significantly different from WT ***$P < 0.0001$ and **$P < 0.002$ by Student's *t* test.